Particle Dispersion and Mixing of Conservative Properties in an Eddy-Resolving Model

CLAUS W. BÖNING

Geophysical Fluid Dynamics Program, Princeton University, Princeton, New Jersey

MICHAEL D. COX

Geophysical Fluid Dynamics Laboratory/NOAA, Princeton University, Princeton, New Jersey

(Manuscript received 14 October 1986, in final form 23 September 1987)

ABSTRACT

We examine the diffusive behavior of the flow field in an eddy-resolving, primitive equation circulation model. Analysis of fluid particle trajectories illustrates the transport mechanisms, which are leading to uniform tracer and potential vorticity distributions in the interior of the subtropical thermocline. In contrast to the assumption of weak mixing in recent analytical theories, the numerical model indicates the alternative of tracer and potential vorticity homogenization on isopycnal surfaces taking place in a nonideal fluid with strong, along-isopycnal eddy mixing.

The eastern, ventilated portion of the gyre appears to be sufficiently homogeneous to allow the concept of an eddy diffusivity to apply. A break in a random walk behavior of particle statistics occurs after about 100 days when along-flow dispersion sharply increases, indicative of mean shear effects. During the first months of particle spreading, eddy dispersal and mean advection are of similar magnitude. Eddy kinetic energy is of O(60–80 $cm^2 s^{-2}$) in the model thermocline, comparable to the pool of weak eddy intensity found in the eastern parts of the subtropical oceans. Eddy diffusivity in the model thermocline ($K_{xx} = 8 \times 10^7$, $K_{yy} = 3 \times 10^7$ $cm^2 s^{-1}$) seems to be higher by a factor of about 3 than oceanic values estimated for these areas. Below the thermocline, model diffusivity decreases substantially and becomes much more anisotropic, with particle dispersal preferentially in the zonal direction. The strong nonisotropic behavior, prominent also in all other areas of weaker eddy intensity, appears as the major discrepancy when compared with the observed behavior of SOFAR floats and surface drifters in the ocean.

1. Introduction

The distributions of conservative properties at sea represent the integrated effect of a broad spectrum of energetic oceanic motions. The investigation of the mechanisms that shape the fields of passive chemical tracers or dynamically active quantities such as potential vorticity is a task of central importance in oceanography.

Cox and Bryan (1984) and Cox (1985) have recently reported on numerical studies of the general circulation, which were directed particularly toward an understanding of flow dynamics of the subtropical wind-gyres. The primitive equation, multilevel models, driven by idealized wind and thermohaline forcing to predict both circulation and stratification, illustrated the competitive action between forced convection interacting with the outcrop zone, and advection and diffusion in formation of the thermocline. The distributions of passive tracers carried by the models and potential vorticity on sigma surfaces were analyzed within the framework of recent analytical theories which built upon conservation of potential vorticity (Luyten et al. (1983); hereafter LPS; Rhines and Young (1982); hereafter RY).

With a coarse, noneddy resolving resolution (Cox and Bryan, 1984), a distinction between a directly "ventilated" zone and a recirculating "pool" zone in the western part of the gyre is visible in the tracer and potential vorticity (q) distributions. A water mass, undergoing convection at the outcrop line, draws a tongue with high tracer values and low q along the isopycnal surface as it is carried southward and westward by the interior flow of the subtropical gyre. The characteristics of this ventilated water are in marked contrast to the poorly ventilated zone of recirculating flow with high values of q, originating at the frontal zone associated with the boundary current.

A high resolution case (Cox, 1985) permitted a substantial reduction of the parameterized diffusivity and led to intense eddy activity within the subtropical gyre. Remarkably, the lateral mixing by the eddies effectively eliminated the front between pool and ventilated zone. A large region with nearly homogeneous q emerged in the interior of the thermocline.

Absence of contrast between regions thought to be

Corresponding author address: Dr. Claus Böning, Institut für Meereskunde an der Universitat Kiel, Düsternbrooker Weg 20, D 2300 Kiel 1, West Germany.

"ventilated" and "unventilated" is in agreement with tritium observations of Sarmiento (1983). Maps of potential vorticity on isopycnal surfaces have recently been constructed for the world's oceans (McDowell et al., 1982; Keffer, 1985) and have begun to serve as a valuable diagnostic for the general circulation (Holland et al., 1984). Reviews of the observational data and discussions of the potential vorticity concept are given by Rhines (1986) and Bryan (1987). One of the interesting features of the observed isopycnal fields are large areas of nearly uniform q found at the base of the thermocline in the subtropical gyre of the North Atlantic and Pacific. They have become a focal point of theoretical approaches toward an understanding of the gyre dynamics.

Rhines and Young pointed out that within an area of recirculating flow, isolated from direct surface forcing, q would be homogenized by lateral eddy fluxes. Luyten et al. advanced the idea of an ideal fluid where q, conserved along the geostrophic contours, is determined by the surface conditions at the outcrop. In this theoretical framework, a uniform distribution of q within the gyre implies a rather uniform q at the source region. Both concepts have in common that they rely on the assumption of a weak lateral mixing. In contrast, Cox's model results suggest the possibility that entering, low q waters are mixed rapidly with the surrounding fluid by an intense eddy activity.

The objective of this study is to elucidate and quantify the transport mechanism in the interior portion of the subtropical gyre. While the model, with its simplified geometry and forcing pattern is not meant to give an accurate simulation of the flow in a particular ocean basin, it essentially combines all the features of the RY's and LPS' theories within an idealized, eddy-resolving, thermohaline ocean. In this sense, the model may serve as a link between theory and reality.

The approach we adopt here to describe the tracer transport mechanism is a trajectory analysis of fluid parcels. The evolution of a mean concentration field is determined by the statistics of single particles (Davis, 1983). The Lagrangian analysis provides a straightforward description of lateral advection and eddy dispersal. It has become a valuable diagnostic of transport processes in meteorological models (Hsu, 1980; Kida, 1983). In recent years some progress has been made in characterizing mesoscale lateral dispersion of the oceanic flow by using quasi-Lagrangian drifting floats (Freeland et al., 1975; Riser and Rossby, 1983; Rossby et al., 1983) and satellite-tracked near-surface drifters (Colin de Verdiere, 1983; Krauss and Böning, 1987). A comparison with the, however still limited, oceanic float observations provides an opportunity to test the validity of the model.

There are, however, some general problems in the application of a Lagrangian analysis to an Eulerian-type, ocean circulation model. Haidvogel (1982; 1984, unpublished manuscript) has pointed out that the uncertainty of model velocities on the grid box scale due to aliasing effects in the treatment of nonlinear terms can lead to a serious accumulation of "errors" in the Lagrangian framework. In general, individual particle trajectories will not be precise enough to allow an evaluation of Lagrangian vorticity or tracer budgets. On the other hand, and reassuringly for the purpose of the present study, these uncertainties were shown to have only little effect on the statistics of an ensemble of particles, i.e., the dispersion behavior.

Another major difficulty concerns the interpretation of Lagrangian statistics in an inhomogeneous flow field, as found especially near the western boundary of an ocean basin. In regions with large gradients of eddy energy, fluid particles will rapidly be swept into different kinematical areas. The rate-of-dispersion or Lagrangian diffusivity will then, in general, depend on the particle spreading time and does not represent a property of the flow field at a given location. The purpose of the present study is not to explore the applicability of the "eddy diffusivity" concept within the context of the entire model flow. The analysis will focus on the dispersion behavior of fluid particles in the interior part of the subtropical gyre. The present model departs from previous eddy-resolving circulation studies in that it uses a basin which is wide enough to allow the representation of large interior areas with rather uniform flow statistics. An analysis of particle spreading in regions away from the western boundary will be a useful starting point in the application of Lagrangian concepts to eddy-resolving circulation models.

Our presentation begins with a short review of the numerical model in section 2. After discussing the recovery of particle trajectories, we will give a qualitative description of particle spreading in different regions of the model domain in section 3. The following quantitative trajectory analysis focuses on particles in the subtropical gyre. In section 4 the (absolute) dispersion of single particles is examined and compared with the mean displacement. Section 5 deals with the Lagrangian diffusivity and its depth dependence in the gyre interior. This includes a test of Taylor's theorem, i.e., the applicability of the concept of homogeneous turbulence in this model region. In the discussion, section 6, we make an attempt to compare the dispersal characteristics with observations of surface drifters and SOFAR floats in the North Atlantic. We conclude with a discussion of the model results in relation to the circulation theories based on the weak mixing assumption.

2. Model background

In the numerical study as reported by Cox (1985) a primitive equation, multilevel model is applied over a rectangular basin of 60 degrees width, extending from the equator to 65°N. The depth is constant (4000 m), except for an idealized shelf and coast along the western

wall. In the vertical, 18 levels are used. The horizontal grid of ⅓° meridional and 0.4° zonal resolution allows the representation of the upper mesoscale range of oceanic eddies. Subgrid scale motions are parameterized by biharmonic lateral mixing terms with 8×10^{18} $cm^4\ s^{-1}$ eddy viscosity and 2.4×10^{19} eddy diffusivity and vertical mixing (10 and 0.3 $cm^2\ s^{-1}$, respectively). The flow is driven by steady zonal wind stress and buoyancy flux utilizing a Newtonian relaxation of surface density toward a specified reference density, linearly increasing with latitude.

After 540 years of integration on a coarser grid to establish the basic density stratification, the fine resolution case was integrated for 24 years, in which the solution became very energetic with mesoscale eddies. Features of the statistical mean solution in the time interval from year 18 to 24 of integration are described and compared to the coarse grid case in Cox (1985). The patterns of the geostrophic mean flow, eddy kinetic energy and tracer on an isopycnal surface (σ = 26.0) are reproduced in Fig. 1. The distribution of the tracer entering along the outcrop (Fig. 1b) is strongly affected by eddy mixing, as a comparison with the coarse-grid, noneddy resolving reference solution (Fig. 1a) reveals. Advection by the mean flow draws a tongue with high tracer (and low q) values toward the south and west. The sharp contrast between the ventilated and the unventilated, "pool" zone of the gyre is effectively wiped out by the eddy activity in the fine resolution case, and a large region with rather uniform tracer (and q) values is established in the interior. The eddy energy shows highest values in the region where the western boundary current leaves the coast. (Maximum values are about 1000 $cm^2\ s^{-2}$ along the axis of the eastward jet.) A band of moderate eddy activity extends across the westward flowing sector of the gyre.

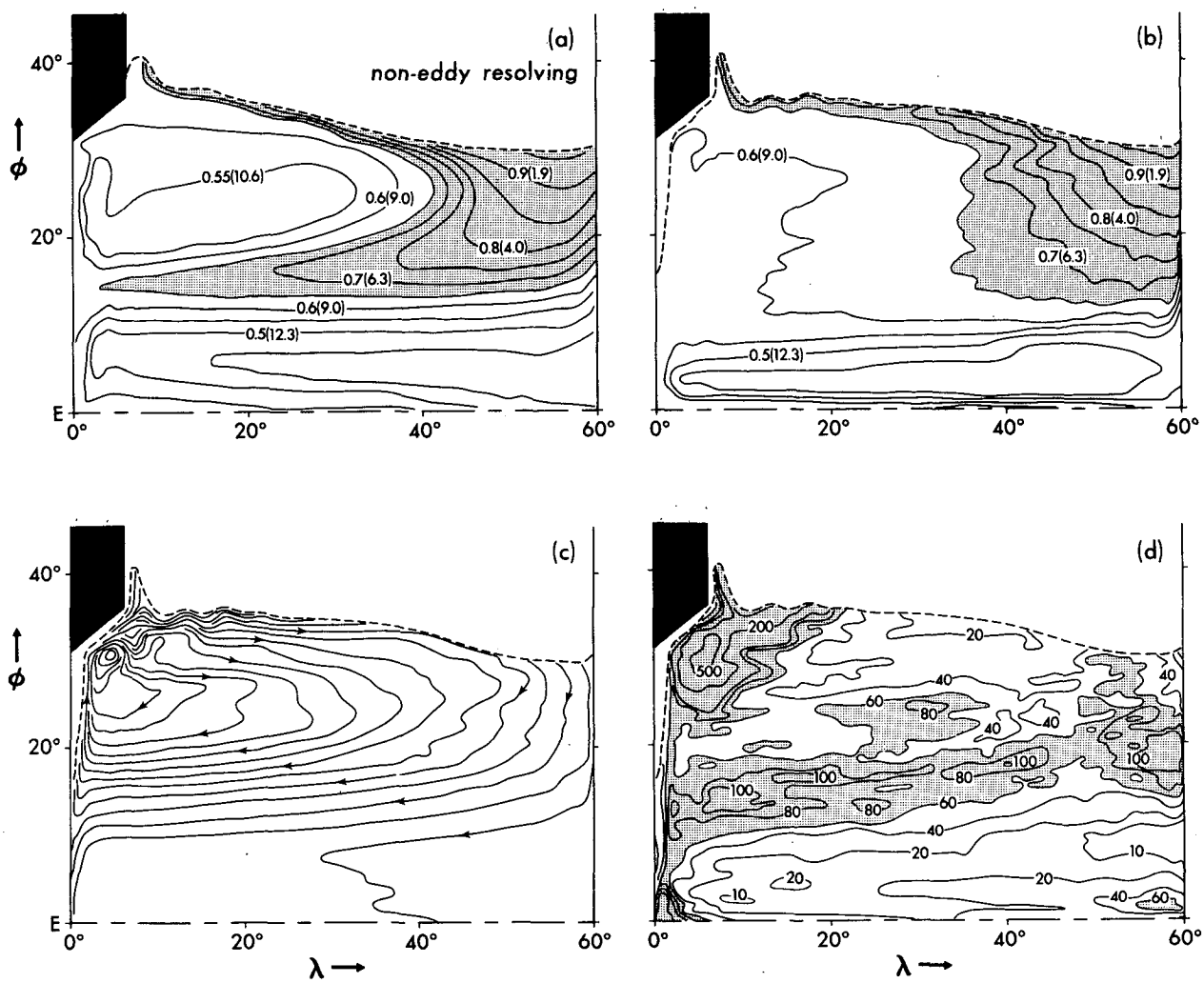

FIG. 1. Six-year mean values evaluated on the σ = 26.0 surface; tracer for the non-eddy-resolving case (a) and for the eddy-resolving case (b); Bernoulli function with contour interval = 5 dyn cm (equivalent vertical displacement) (c); eddy kinetic energy in units of $cm^2\ s^{-1}$ (d) (reproduced from Cox, 1985).

Figure 2 gives a snapshot of the flow in this area. The instantaneous flow in the gyre interior is dominated by mesoscale structures with a predominant scale of 200 km. The biharmonic mixing is effective in suppressing smaller scale features. On the other hand, Cox (1987) demonstrated that nonlinear interactions in the eddy field lead to a significant transfer of energy into low-frequency, larger-scale zonal motions. We will see the effect of these, predominantly barotropic fluctuations in the particle dispersion characteristics, especially below the thermocline.

3. The Lagrangian view

a. Recovery of particle trajectories

When attempting to extract Lagrangian information from an inherently Eulerian dataset, care must be taken that computational errors remain small compared to the amplitude of the derived quantity of interest. The task at hand is to establish simulated particle trajectories from a given velocity field. To accomplish this, the equation

$$d\mathbf{x}(t, p)/dt = \mathbf{u}(\mathbf{x}(t, p), t) \qquad (3.1)$$

must be integrated numerically, where particles are identified by the parameter $p = 1, 2, \cdots$, and the vectors $\mathbf{x}$ and $\mathbf{u}$ give the 3-D particle positions and velocities. Various potential problems exist in applying this equation to the Eulerian velocity field from the model. Haidvogel (1982) has pointed out that the computed trajectories can be quite sensitive to the details of the algorithm used, although such sensitivity may be expected to be small when variability of velocity, both temporal and spatial, is well resolved in the available data.

Two tasks are involved in implementing (3.1) numerically. The velocity, $\mathbf{u}$, must be established at a point in space and time which is, in general, positioned between available data points. Second, the time derivative must be evaluated in a manner to assure accuracy. The latter problem will be addressed first. There are various schemes available for conducting numerical integration of differential equations of the type of (3.1). These range from computationally quite simple algorithms to complex iterative schemes. The latter yield improved accuracy for a given timestep. However, the simpler schemes can be made highly accurate as well, by taking sufficiently small timesteps. We have chosen to use the simple Euler scheme here, in which the particle position at the new timestep is calculated directly from the velocity at the position of the present timestep. Since this scheme is only accurate to first order in time, we must take quite short timesteps to avoid significant truncation error. In practice, we have scaled the timestep to the gridspace resolution by requiring that the particle undergo at least n steps to proceed from one side of a grid box to the opposite side. That is, the timestep shortens as the ambient velocity increases. To assure accuracy, we have run several tests, recomputing given trajectories using increasing n, until no further significant change is seen in the trajectory. This point is reached at $n = O(100)$ and we have adopted $n = 200$ for this study. Comparing typical trajectories computed using $n = 200$ and $n = 400$, we find changes of less than 1% in final particle position between the two for each of the three dimensions, when compared to total particle displacement in the respective dimension.

The job of establishing velocities between given time and grid points is more difficult. The data is provided at a time interval of 3 days, which resolves the temporal variability of the solution quite well. Therefore, linear interpolation between the given time points provides an accurate recovery of actual time dependence. The

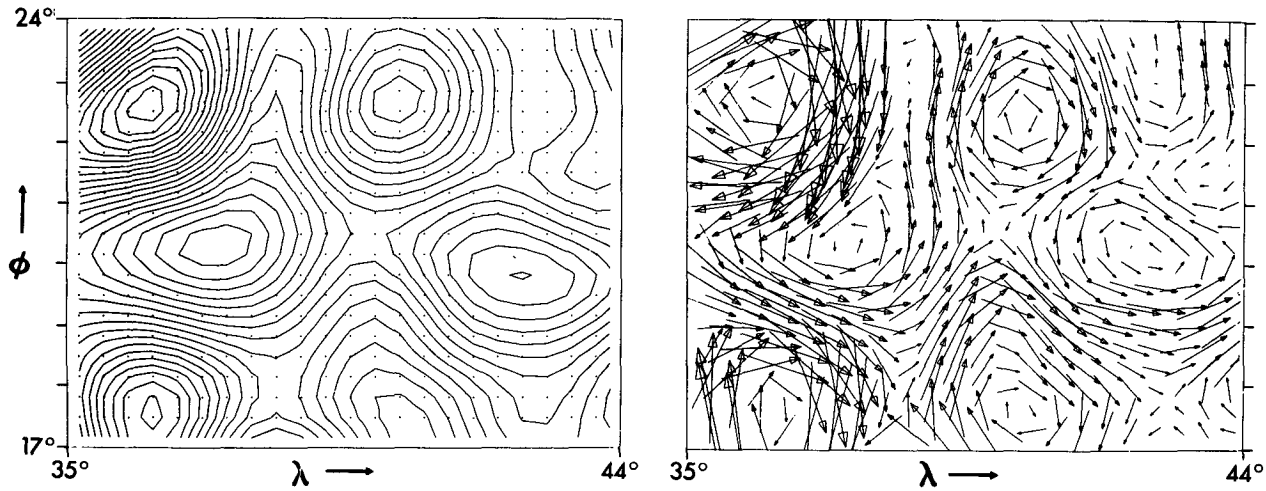

FIG. 2. Instantaneous flow field in the westward flowing sector of the subtropical gyre. Left: Streamlines of the external component with contour interval = 5 Sv. Right: Velocity vectors (drawn at the grid points) in the thermocline; a vector of 1° length corresponds to 10 cm s^{-1}.

spatial problem is, however, more difficult due to an arbitrariness involved in determining quantities between gridpoints. An obvious choice is linear interpolation, as is done in time. Higher level interpolation is also an option. However, one may argue that a given gridpoint velocity represents velocity at all points within its own grid box and, therefore, a velocity between gridpoints should be given as that of the nearest gridpoint. Since, in the opinion of the authors, no one of these schemes is clearly more appropriate than the others, one can only wish to show that the overall results of the study, which are based upon the computed trajectories, are not expected to be unacceptably sensitive to the particular technique used. Toward this end, we have computed many of the trajectories upon which the most central of the findings of this study are based, using linear interpolation first, and then the nearest-gridpoint scheme described here. Diffusivities computed from the two datasets are found to differ by less than 10% between the two, well within error bars established later and arising due to unrelated effects. This relatively low degree of sensitivity affirms that the principal scales of spatial variability within the velocity field are generally well resolved by the gridspace. We have chosen linear interpolation between the eight adjacent gridpoints for this study.

We are thus provided with a dataset consisting of time series of particle velocities

$$\mathbf{u}_p(t) = [u_p(t), v_p(t), w_p(t)]$$

and particle trajectories

$$\mathbf{x}_p(t) = [x_p(t), y_p(t), z_p(t)].$$

In the statistical analysis we consider only the horizontal components; i.e., we examine the projections of the 3-D trajectories on a level surface. Due to the small aspect ratio of the oceanic flow, the difference between the horizontal projection of dispersion and the actual, approximately along-isopycnal, dispersion is negligible.

b. *Examples of particle behavior*

Before proceeding with a quantitative examination of Lagrangian statistics in the interior of the subtropical gyre, this section is intended to provide a qualitative picture of the particle behavior under various flow conditions.

Figure 3 illustrates two different types of the lateral spreading of particles in different flow regimes. The particles are seeded simultaneously on 12×12 neighboring grid points. Their positions are shown as projections on a horizontal plane with respect to their initial locations as a function of time. The first case, actually representing a cluster in the subpolar region, is quite characteristic of particle behavior in areas where eddy energies are very weak. The other case represents an example of particle spreading in the moderate eddy field of the subtropical thermocline. There is only a weak displacement of the center-of-gravity of the particle cluster in the first example ($\bar{u} = 0.7$, $\bar{v} = 0.05$ cm s^{-1}), whereas the ensemble in the subtropical gyre is moved toward the west, indicative of the westward mean flow ($\bar{u} = -8.4$, $\bar{v} = -2.2$ cm s^{-1}). More interesting is the difference in particle dispersion relative to the center-of-gravity as caused by the turbulent nature of the flow field. In the weak eddy field ($\overline{u'^2} = 21$, $\overline{v'^2} = 19$ cm^2 s^{-2}), particle dispersion is strongly anisotropic with large zonal and small meridional displacements, whereas it is more isotropic in the stronger eddy field of the subtropical gyre ($\overline{u'^2} = 74$, $\overline{v'^2} = 62$ cm^2 s^{-2}). Below the subtropical thermocline, the behavior resembles case (a), meridional excursions are very small and particles spread preferentially in the zonal direction.

The behavior of passive tracers over longer time periods is illustrated by Fig. 4 showing particle spreading in the subtropical thermocline. Particles are started at a level close to the $\sigma = 25.75$ surface. (The outcrop line of this surface lies slightly to the south of the 26.0 surface shown in Fig. 1.) In the first example Fig. 4a, a cluster of particles with initial location at the northern rim of the subtropical gyre is tracked. Initial streakiness of the particle cloud, with spiraling arms reaching far out laterally 0.5 and one year after release, is followed by more uniform distributions after longer times. Inspection of the vertical component of the position vectors indicated that particles tended to follow the bowl-shaped isopycnal surface. After two years, particles occupy a large fraction of the subtropical gyre. At that time, some have completed a full circuit and are carried by the central jet toward the east again. Only a few have escaped the subtropical gyre northward by leaking out along the western wall. Over the whole period, particle motion is strongly dominated by the turbulent spreading of the cloud which masks the "mean" motion of the ensemble.

The second example (Fig. 4b) shows the fate of a group of particles released in the eastern part of the thermocline. An advective component is more visible in this case, but again turbulent spreading is substantial while the ensemble is carried toward the west in the Sverdrup return flow, and appears to be comparable in magnitude to the mean component. The spreading of particles illustrates the way conservative properties are mixed within the model flow.

Obviously, there are many particle seeding and sampling strategies which can be imagined for a Lagrangian analysis of a model flow field (or the oceanic flow). Any choice has to be a compromise between the large amount of float data which is required to establish stable statistics in a given area of the flow, and the constraints imposed by computational considerations. The strategy adopted here is oriented towards getting a large number of float days in a few selected areas, rather than a uniform distribution over the model basin. Groups of 144 particles each are simultaneously

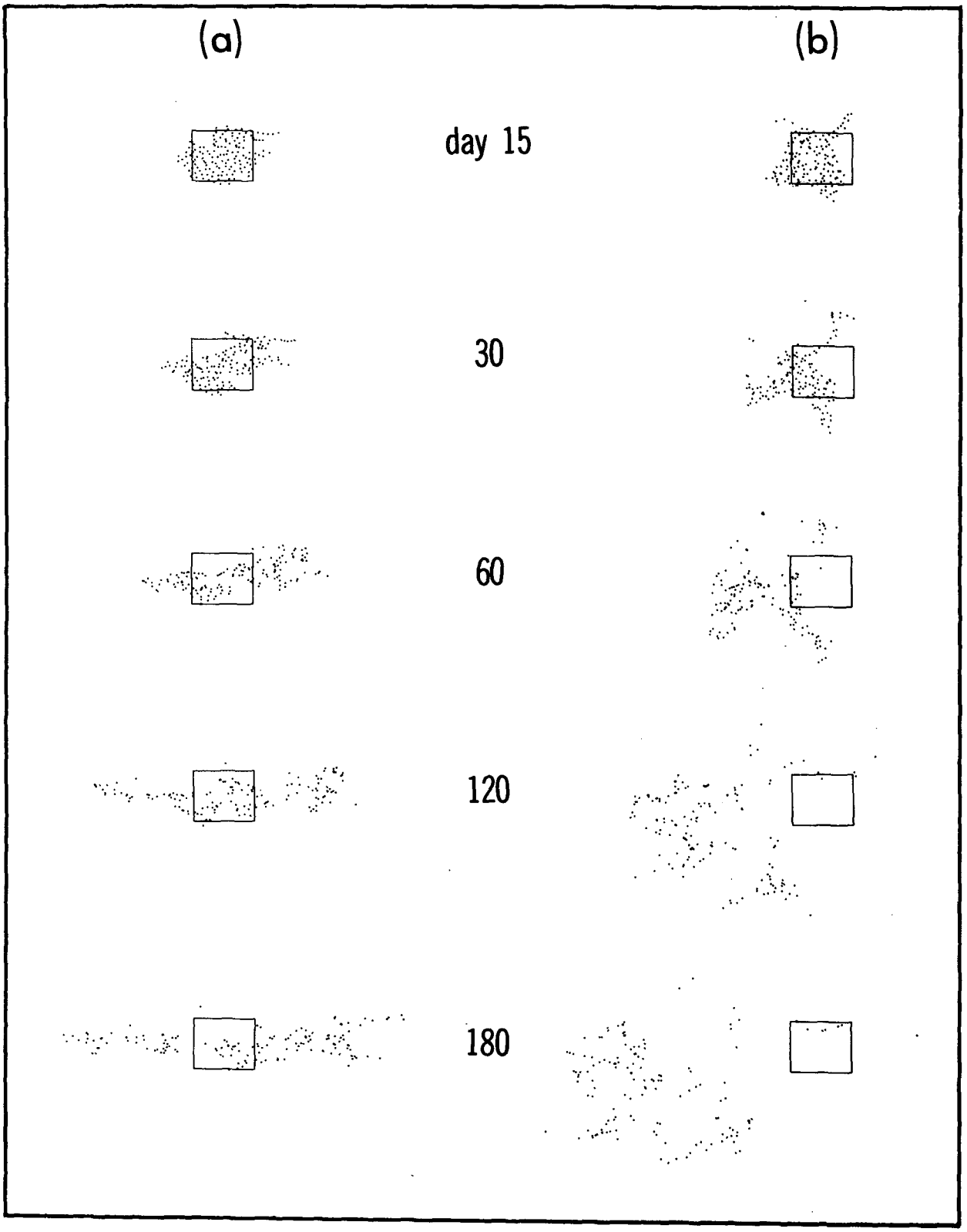

FIG. 3. Examples of particle behavior: positions at five points of spreading time, relative to the initial location (rectangles), starting level 90 m, group (a) in a region of very weak eddy energy, group (b) in the moderate eddy field of the subtropical thermocline.

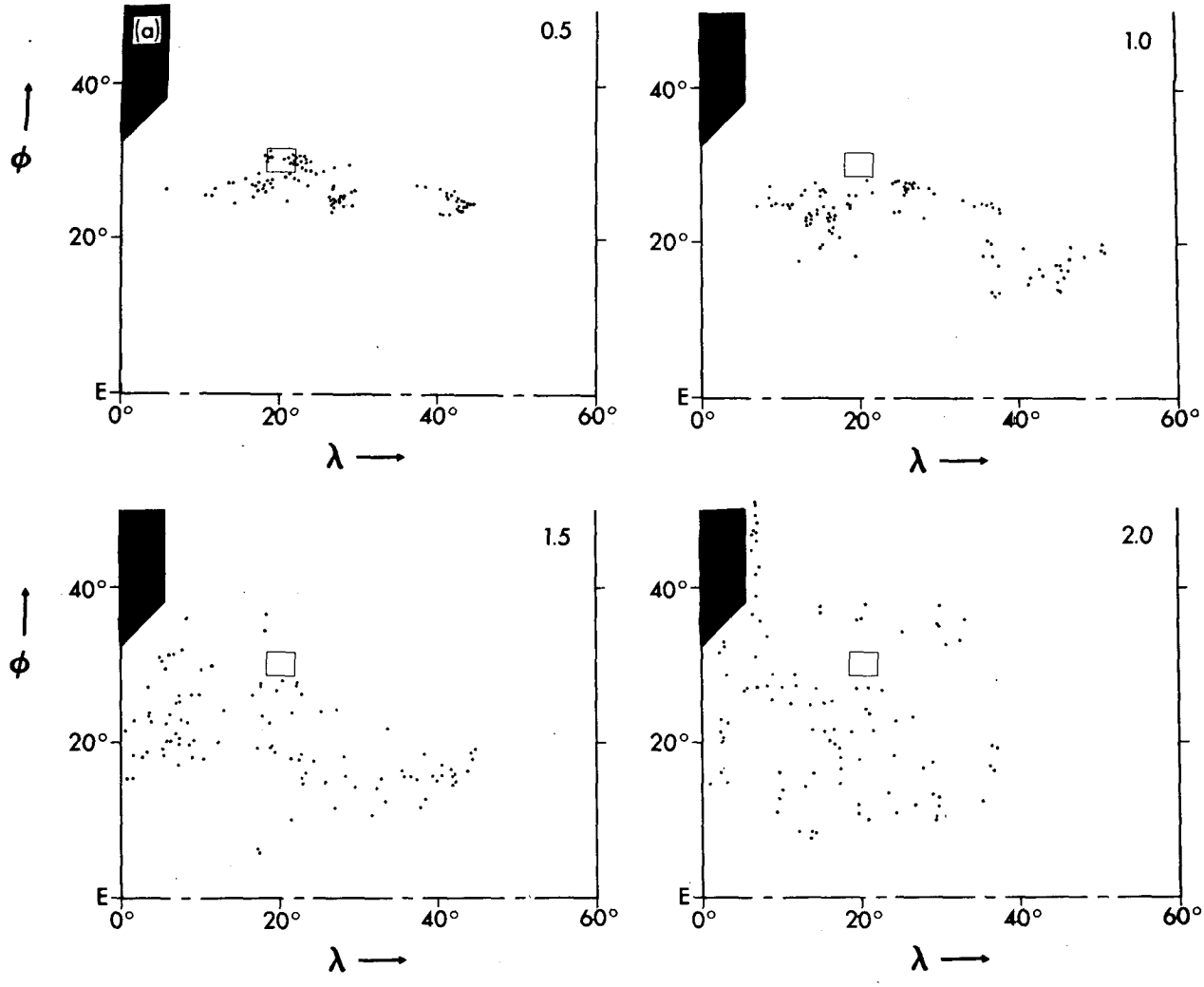

FIG. 4. Particle spreading in the subtropical thermocline over a period of two years; initial locations are indicated by the rectangles.

released, at several times between model years 18 and 24, in all 18 model levels. At the beginning of the experiments, the particles of a group occupy 12 × 12 neighboring gridpoints (Fig. 5). The starting areas have been chosen with respect to the homogeneity of the Eulerian statistics, in order to assure uniform flow conditions for spreading times as long as possible. Of particular interest in the following analysis will be the behavior of particles in the westward moving sector of the subtropical gyre. The group denoted "A" in Fig. 5, analyzed in detail, will serve as a prototype.

4. Particle dispersion

Instead of the trajectories, $\mathbf{x}(t, p)$, we now consider the lateral displacements of particles during a time period τ. Under the assumption of stationary statistics, the vector of individual particle displacements is $\mathbf{r} = \mathbf{r}(\tau, p)$ and given by

$$\mathbf{r}(\tau, p) = \mathbf{x}(t + \tau, p) - \mathbf{x}(t, p). \tag{4.1}$$

Important characteristics of particle displacement are provided by its first and second moment, completely describing it if the particle probability density is normally distributed (see e.g., Monin and Yaglom, 1971; Davis, 1983). With angle brackets we will denote an ensemble average over all marked particles $p = 1, 2, \cdots, N$ within a group ($N = 144$). The mean $\langle \mathbf{r}(\tau) \rangle$ represents the displacement of the center-of-gravity of a particle ensemble. The dispersion of particles as caused by the turbulent character of the flow is described by the displacement covariance tensor

$$D_{ij}(\tau) = \langle r_i'(\tau) r_j'(\tau) \rangle \tag{4.2}$$

where $r' = r - \langle r \rangle$ are individual particle displacements relative to the mean motion of the ensemble.

The dispersion of particles about their ensemble mean displacements provides a direct view of the rel-

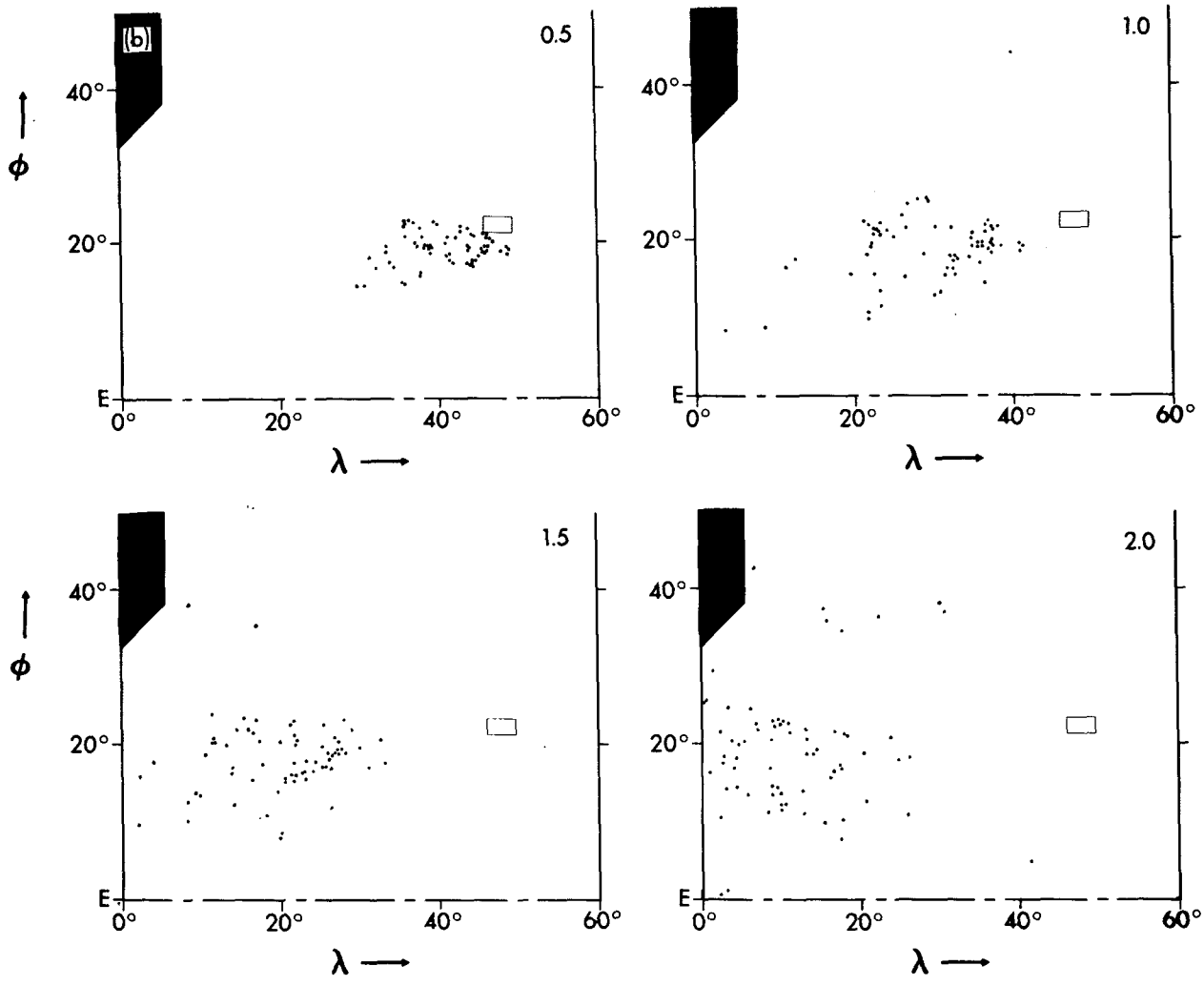

FIG. 4. (*Continued*)

ative influences of mean advection and eddy dispersal on the spreading of a passive tracer in the fluid. To illustrate these competitive effects, Fig. 5 displays the mean component and the principal axes of the covariance tensor of particle displacement for various groups started near the surface. After six months, both mean and eddy component are almost equally important for property transport in the eastern part of the gyre. The dispersion is slightly anisotropic, with the main axis of the covariance tensor tending to orient in the mean flow direction.

The vertical dependence of these components in group A is schematically displayed in Fig. 6. The contribution of mean advection decreases vertically much more rapidly than eddy dispersal, thereby increasing the relative importance of the latter component on total particle spreading. A second feature is a growing anisotropy in particle dispersion with depth.

A simple, quantitative measure of the relative importance of mean advection and eddy dispersal on total property transport may be given by the ratio of mean to rms-particle displacement; i.e.

$$b_i(t) = \frac{|\bar{U}_i|t}{D_i^{1/2}},$$

where $i = 1, 2$ denote the components in the direction of the principal axis of the covariance tensor, or

$$B(t) = \frac{|\bar{\mathbf{U}}|t}{(D_1^{1/2} \cdot D_2^{1/2})^{1/2}}$$

if we are looking at total spreading. Note the time dependency of this quantity: as we will discuss later, in the Taylor limit $D^{1/2}$ would grow like $t^{1/2}$; thus after longer times the advective component becomes more and more dominant. Analogous information is given by the conventional Péclèt-number Pe = UL/K in the Eulerian framework with the dependence on the length scale L.

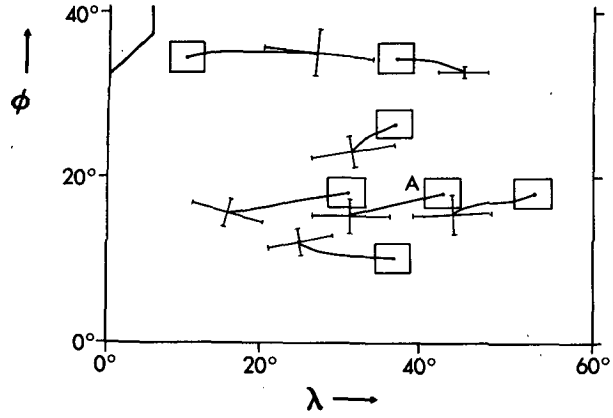

FIG. 5. Ensemble mean displacement over six months and principle axes of the displacement covariance tensor, $D^{1/2}$ after six months of particle spreading. Initial locations of particle groups are indicated by the rectangles; starting level 90 m.

Figure 7 indicates displacements by the mean flow and eddies in the subtropical gyre (group A), and their ratio b_i as a function of time. One may see the slowly growing importance of the mean component as time progresses. The depth dependence of B after six months of spreading is displayed in Fig. 8. Here, the values at each level represent an average of ten realizations, with

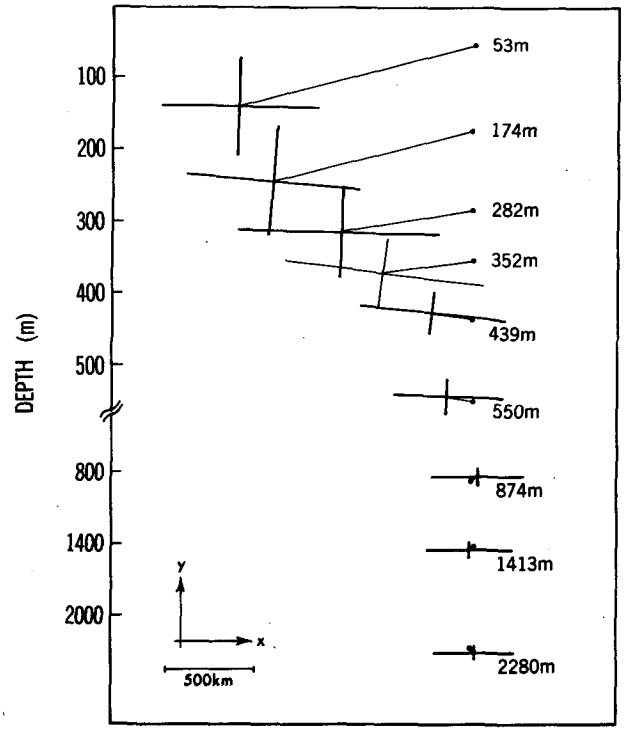

FIG. 6. Ensemble mean displacement (time-averaged) and principal axes of displacement covariance ($D^{1/2}$) for particles started in various depths in the subtropical gyre (group A).

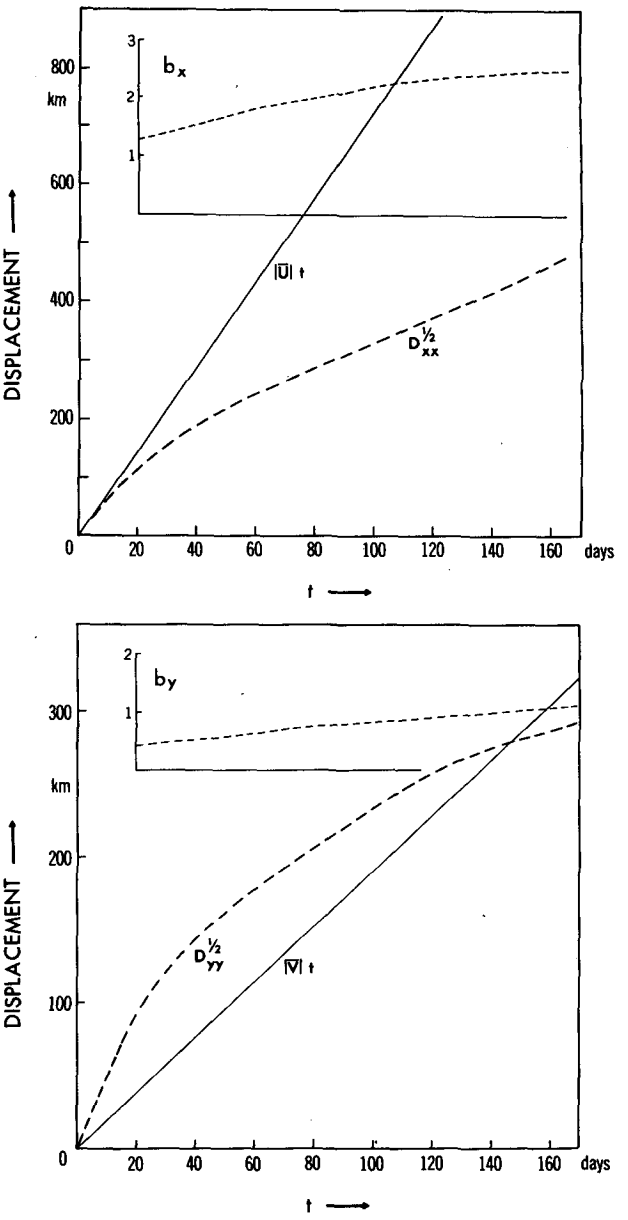

FIG. 7. Particle displacement by the mean flow, $|U_i|t$, by the eddies, $D_i^{1/2}$, and their ratio b_i as functions of time in the subtropical thermocline (group A); starting levels 90 m (a), 351 m (b).

ensembles of 144 particles released at different times during model years 18–24. We note again the relative importance of mean advection to drop strongly in the thermocline, from near surface values of $B \sim 3$ to middle depth minima less than 1. We complement this by giving the Péclèt number Pe (based on the diffusivities as derived in section 5). The local values, taking $L = 300$ km, and the vertical dependence are similar to B in the thermocline. It should be noted, however, that the precise meaning of the scale L is dubious, whereas the time scale in B has a clear definition.

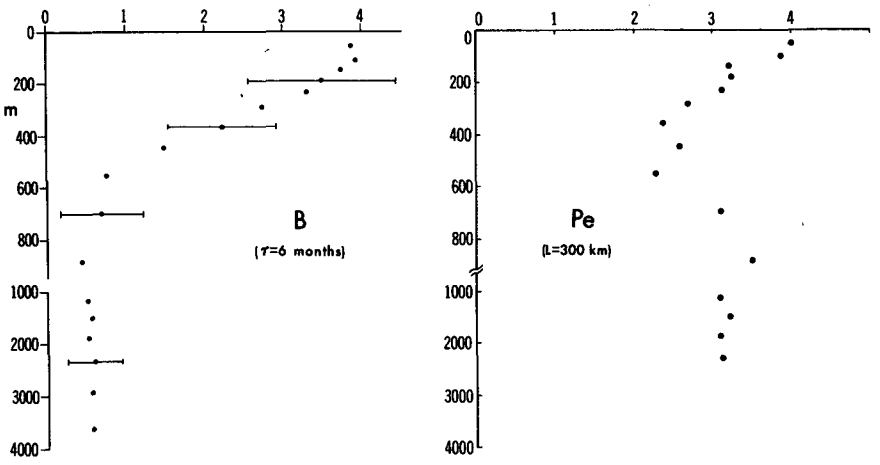

FIG. 8. The ratio of mean to eddy displacement B and the Péclèt number Pe = UL/K as functions of depth in the subtropical gyre (group A); here, U is the mean Eulerian velocity in the area covered by the particles, and K represents the apparent diffusivity discussed in section (c).

5. Lagrangian diffusivity

a. Theoretical considerations

The time-rate-of-change of single particle dispersion defines the Lagrangian diffusivity

$$K_{ij} = \frac{1}{2}\frac{d}{dt} D_{ij} \qquad (5.1)$$

Under general flow conditions, K is a function of spreading time which precludes an interpretation in a Eulerian sense; i.e., it cannot be interpreted as an "eddy diffusivity" of the flow at a given location.

In the case of stationary and homogeneous turbulence, the dispersion of particles is related to their Lagrangian velocity autocorrelation through

$$D_{ij}(\tau) = (\overline{u_i'^2}\,\overline{u_j'^2})^{1/2} \int_0^\tau (\tau - s)[R_{ij}(s) + R_{ji}(s)]ds \quad (5.2)$$

(Batchelor, 1949). This identity was first shown by Taylor (1921) for the case of isotropic turbulence; we refer to (5.2) as "Taylor's Theorem." The correlation function

$$R_{ij}(t) = \frac{1}{\overline{u_i'^2}\,\overline{u_j'^2}} \left\langle \frac{1}{T_{\max}} \int_0^{T_{\max}} u'(t, p)u'(t + \tau, p)d\tau \right\rangle, \quad i, j = 1, 2 \quad (5.3)$$

is subject to the definition of the mean velocity

$$\overline{u_i} = \left\langle \frac{1}{T} \int_0^{T_{\max}} u_i(\tau, p)d\tau \right\rangle$$

so that individual fluctuations are

$$u_i'(\tau, p) = u_i(\tau, p) - \overline{u_i}.$$

The velocity variance is given by

$$\overline{u_i'^2} = \left\langle \frac{1}{T_{\max}} \int_0^{T_{\max}} u_i'(\tau, p)u_i'(\tau, p)d\tau \right\rangle.$$

Moving within the turbulent flow, particle velocities eventually become decorrelated from the starting velocities. This memory loss is characterized by the Lagrangian integral time scale

$$T_i = \int_0^\infty R_{ii}(\tau)d\tau$$

which, if it exists, is a measure of the time period after which the particle velocities become decorrelated. The distance which particles move during this period may then be given by

$$L_i = \overline{u_i'^2}^{\,1/2}\, T,$$

characterizing a "mixing length" of the turbulent flow.

From (5.2), two limiting relations emerge resulting from $R = 1$ at $\tau = 0$ and $R \to 0$ for very large τ (consider $i = j$):

$D_{ii}(\tau) = \overline{u_i'^2}\tau^2$ for $\tau \ll T$, the initial dispersion,

$D_{ii}(\tau) = 2\overline{u_i'^2}T\,\tau$ for $\tau \gg T$,

the random walk regime.

The diffusivity therefore will become constant, given by the velocity variance and the time scale, $\overline{u'^2}T$, or equivalently, $\overline{u'^2}^{\,1/2}L$, where L represents the length scale $L = \overline{u'^2}^{\,1/2}T$.

The significance of the homogeneous case lies in the fact that the Lagrangian diffusivity K is related to the Eulerian "eddy diffusivity." In the Eulerian framework, turbulent diffusion of a passive admixture with concentration $\theta(x, t)$ is described by the eddy flux of θ

which often is *assumed* to be related to the mean gradient of θ by

$$-(\overline{u_i'\theta'}) = A_{ij}\frac{\partial}{\partial x_j}\bar{\theta}, \tag{5.4}$$

defining an eddy diffusivity tensor A_{ij}.

Finding the mean concentration θ of a passive tracer is equivalent to determining the probability density for the position x of a fluid particle (Monin and Yaglom, 1971). Under the assumption of a Gaussian distribution which is justified in statistically homogeneous flow, it is completely described by the first and second moment of particle displacement. Thus, if mean scalar transport were described by a linear flux-gradient law (5.4), then particle displacement covariance had to increase linearly with time, and single particle dispersion would determine diffusive transport in the mean distribution of scalar properties (Davis, 1983). Thus, modeling turbulent diffusion by a "diffusion equation" implies a relation between the turbulent diffusivity A and the second moment of particle displacement. However, whereas the definition (5.1) applies in the general case, the validity of an "eddy diffusivity" concept strongly depends on the assumption of homogeneity.

b. *The assumption of homogeneity*

The applicability of (5.4) and, equivalently, the existence of a constant random walk diffusivity which may be identified as "eddy diffusivity" of the flow in a certain area, critically depend on the homogeneity of the flow field. The limitations of the approximation (5.4) have often been noted (e.g., Corrsin, 1974): Evolution of the mean field follows a flux-gradient law only over times long compared with the Lagrangian decorrelation time. The turbulence length scale must be much smaller than the distance over which the curvature of the mean transported field changes appreciably.

From the pattern of eddy kinetic energy in an ocean basin it is apparent that in many regions the assumption is fundamentally wrong. This is especially the case near the western boundary where the eddy diffusivity concept may not make any sense at all. (Assuming quasi-homogeneity in small enough areas, or, focusing on short particle spreading periods may provide no way out of the dilemma due to the conditions mentioned here.) Harrison (1978) showed that the eddy diffusion model does not satisfactorily describe the eddy fluxes in any region of a particular numerical circulation model. The model basin was rather small (2000 km $\times$ 2000 km) in that case and eddies were generated only in the intense recirculation of the eastward jet.

The situation seems to be more favorable in our main area of interest, the interior of the subtropical gyre. The model basin is wide enough, as the real oceans, to accommodate a broad interior region of relatively weak mean flow without substantial shear. The model eddy field is characterized by a band of moderate intensity with weak gradients in the direction of the mean flow. In the following, we give some simple tests to determine to what extent the homogeneity assumption can be applied. We focus on group A in the westward flowing part of the gyre. The examples shown are based on a single realization, i.e., on the trajectories of 144 simultaneously released particles.

The first question we ask is over which time period it makes sense to regard particle trajectories as being in the same kinematical regime, i.e., for how long will the Lagrangian velocity correlation function be meaningful. Figure 9 shows R_{xx} and R_{yy} according to (5.3), defined for three different T_{max}. For both components there are only small differences between the curves. The integral time scales remain fairly constant, T_x = 12.9, 13.0, 13.0 and T_y = 8.8, 8.9, 8.0 days. In this respect, effects of inhomogeneity seem to be negligible for periods up to 150 days.

If flow conditions were approximately homogeneous, we should expect Taylor's theorem to hold. In Fig. 10 the diagonal components of the displacement covariance tensor are depicted as a function of time after

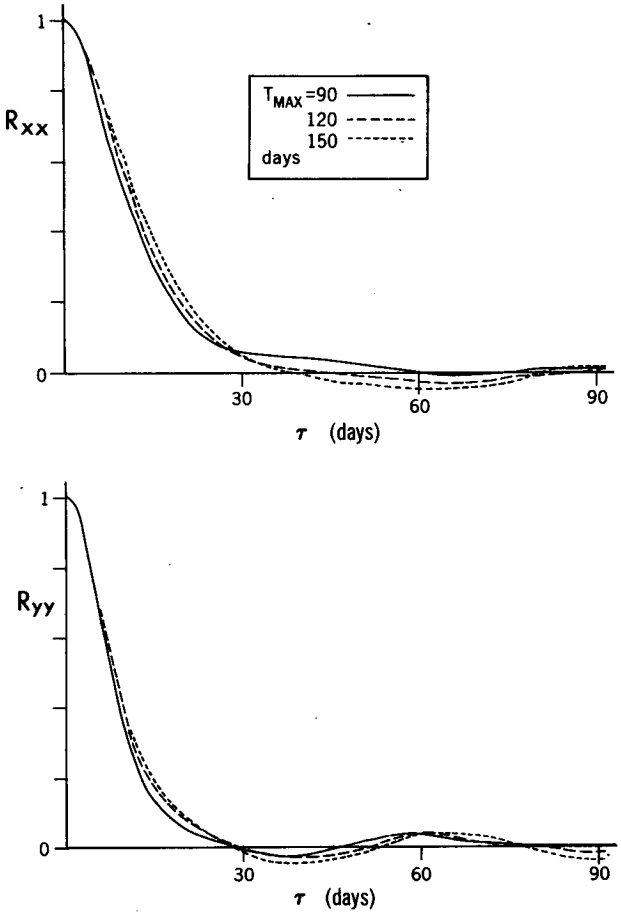

FIG. 9. Lagrangian velocity autocorrelation functions R_{xx} and R_{yy} for three different T_{max} (group A).

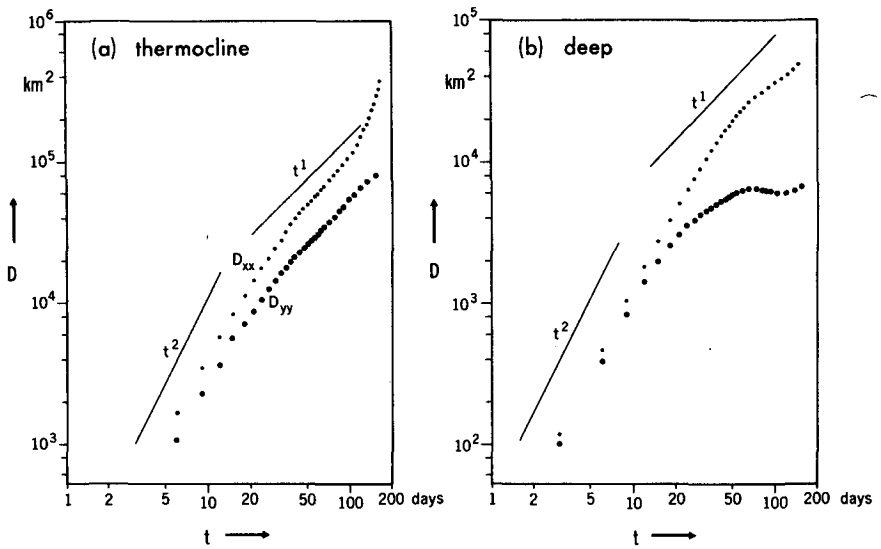

FIG. 10. Components D_{xx}, D_{yy} of the particle displacement covariance tensor as functions of time (group A), near the surface (90 m starting level), and below the thermocline (1414 m).

deployment, for groups in the upper thermocline and below the thermocline. Heavy lines indicate the power laws of the two ranges according to the theory of homogeneous turbulence. The D_{xx} and D_{yy} show good agreement with the expected $\propto t^2$ behavior during the first days. Dispersion slows down then and, in the shallow levels, shows a general tendency toward a random walk behavior after about 30 or 40 days for the zonal, and after 20 or 30 days in the meridional component. A deviation occurs in the zonal component after about 100 days, with a strongly increased rate-of-dispersion. The deep particles show a random walk type behavior with respect to zonal, but a different behavior with respect to meridional dispersion which completely saturates, leading to a strong anisotropy in particle displacement.

As a test of the theorem (5.2), in Fig. 11 we compare the Lagrangian diffusivity as derived directly from particle dispersion, $K(t) = \frac{1}{2}d/dtD(t)$, with the "diffusivity" as calculated from the autocorrelation function,

$$K^*(t) = \overline{u'^2} \int_0^t R(s)ds.$$

In the thermocline, the diffusivities exhibit a marked transition from an initial linear increase to more time-independent values after about 30 days. Consistent with the negative lobes in the velocity correlation functions, the deep diffusivities decrease during some period before approaching a random walklike behavior. Both K_{yy} and K^*_{yy} are approximately zero after about 80 days. We may note a good agreement between the actual and predicted curves for almost the whole period, except for the zonal diffusivity in the thermocline. After about 100 days, a break in the random walk behavior occurs and K_{xx} begins to rise sharply.

An enhanced dispersion in the direction of the mean flow would be expected as an effect of lateral shear of the flow. The influence of a constant mean shear, $\Gamma = dU_1/dx_2$, upon the downstream dispersion of particles has been treated by Corrsin (1959) and Riley and Corrsin (1974). The most prominent feature of the theory is a t^3-dependence as the long-time effect of shear on the variance of fluid particle displacement in the direction of the mean flow,

$$D_{11}(\tau) \to \frac{2}{3}\Gamma^2 T_2 \overline{u_2^2}\tau^3,$$

that is, it increases with time significantly more rapidly than the variances of the transverse diplacements, asymptotically proportional to t. The existence of the asymptotic t^3-dependence has been demonstrated by Deardorff and Peskin (1970) with a numerical model of plane Poiseuille flow at large Reynolds numbers.

We certainly cannot expect this approximate expression to be exactly valid in the case of more complicated flows as in the present model. Nevertheless, one may take the long-time deviation from a random walklike behavior of homogeneous turbulence as seen in the zonal, alongflow component as an indication of shear effects. This break in the random walk behavior limits the applicability of the concept of a constant eddy diffusivity, in this particular case, to about 100 days.

c. *Eddy diffusivity in the eastern subtropical gyre*

The diffusivity values we will present here are obtained as averages over 10 realizations, i.e., 10 groups "A" released at different times within a six-year period in all model levels. In each realization, an apparent

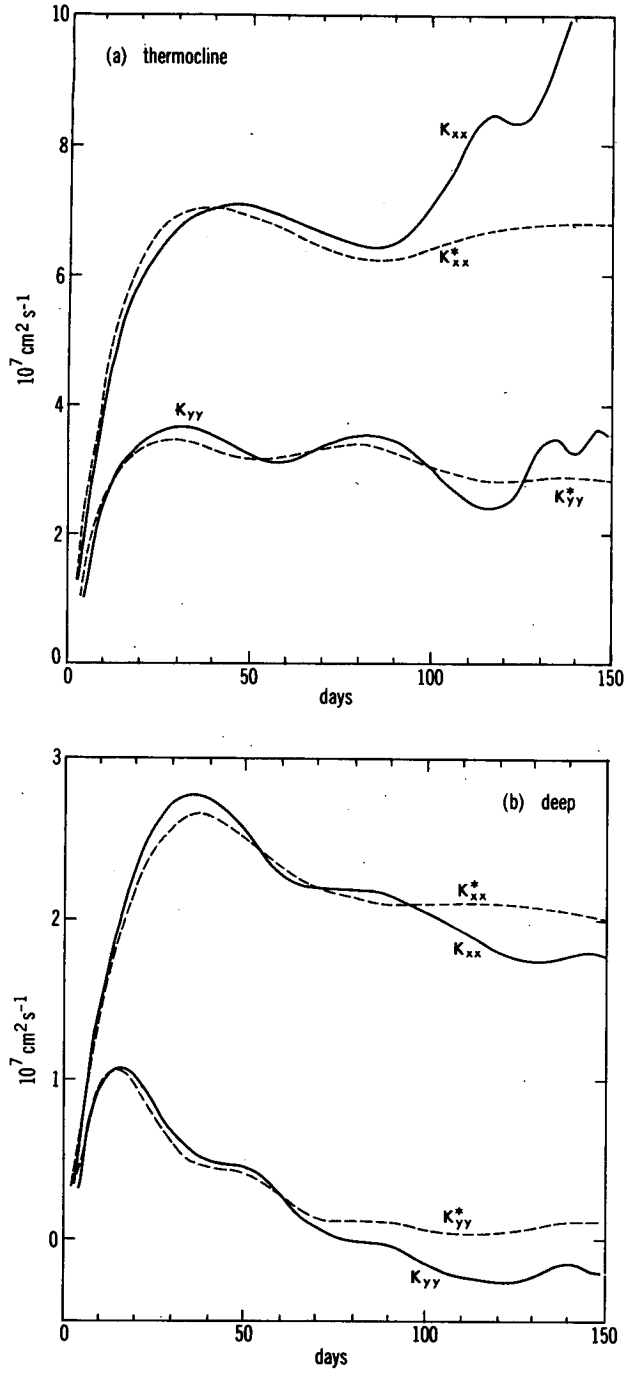

FIG. 11. Lagrangian diffusivity $K(t)$, compared with calculated $K^*(t)$ from velocity correlation according to Taylor's Theorem (group A).

diffusivity is defined as a time mean value of $K(t)$ between days 40 and 100 which is assumed to represent approximately the random walk period.

In Fig. 12 the averages of these realizations are displayed as a function of depth. The error bars represent the standard deviation given by the last averaging procedure and shall give an indication of the variability in time. The profiles of K_{xx} and K_{yy} may be compared with the vertical pattern of velocity variance. Maximum values are found in the thermocline with K_{xx} = 7–8 ($\times 10^7$), $K_{yy} \sim 3 \times 10^7$ cm^2 s^{-1}. Below, both components decrease and eventually take on depth independent values [$K_{xx} \sim$ 2–3 ($\times 10^7$ cm^2 s^{-1})]. The decrease of K_{yy} is much stronger than of K_{xx}. The deep values of K_{yy}, 0–2 ($\times 10^6$ cm^2 s^{-1}), are not significantly different from zero. Particle spreading is strongly anisotropic in the deeper layers, with particle paths oriented zonally.

This behavior is illustrated also in the structure of the autocorrelation functions. Figure 13 shows R_{xx} and R_{yy} for a thermocline and a deep level (one realization only). In the shallow level, zonal and meridional correlation functions are only slightly different and decrease exponentially toward zero. Below the thermocline, substantial differences exist between the components with prominent oscillations in R_{yy}.

The contrasting behavior can be interpreted as a manifestation of the relative influences of turbulent and wavelike character of the fluctuating flow. Due to the β-effect, meridional particle excursions can be effectively suppressed compared to zonal dispersion (Holloway and Kristmannsson, 1984). Examining particle dispersion in a model of homogeneous turbulence on a β-plane, Haidvogel (1984, unpublished manuscript) demonstrated the strong effect of the planetary vorticity gradient in providing unbounded zonally oriented paths for conservative fluid motion with subsequently enhanced (suppressed) particle dispersion in the zonal (meridional) direction. In the presence of pure two-dimensional turbulence, i.e., sufficiently strong rms-velocities, R_{uu} and R_{vv} smoothly decreased with time. As rms-velocities were decreased, the importance of Rossby wave influences emerged and the correlation functions showed substantial anisotropy.

The existence of quasi-steady zonal Eulerian bands of flow in the present model is demonstrated by Cox (1987). These bands arise in regions of high eddy activity and radiate away, filling almost the entire basin. In terms of this analysis, we may view the particle displacements as a result of the combined action of "mean" flow, eddies and the lower-frequency motions of bandlike character. While the eddies may dominate particle motions in the main instability regions, the influence of the zonal bands will be felt more strongly in the quieter parts of the basin. The change of particle statistics with depth in the subtropical gyre appears in this context as a consequence of the more barotropic nature of the bands as compared to the more baroclinic nature of the eddies. As the bandlike structure of the low-frequency motions can be explained as an effect of the mean vorticity gradient, i.e., wave dynamics, on the red energy cascade in the barotropic mode, this view is consistent with the picture of particle behavior in wavelike and turbulent flows as outlined above.

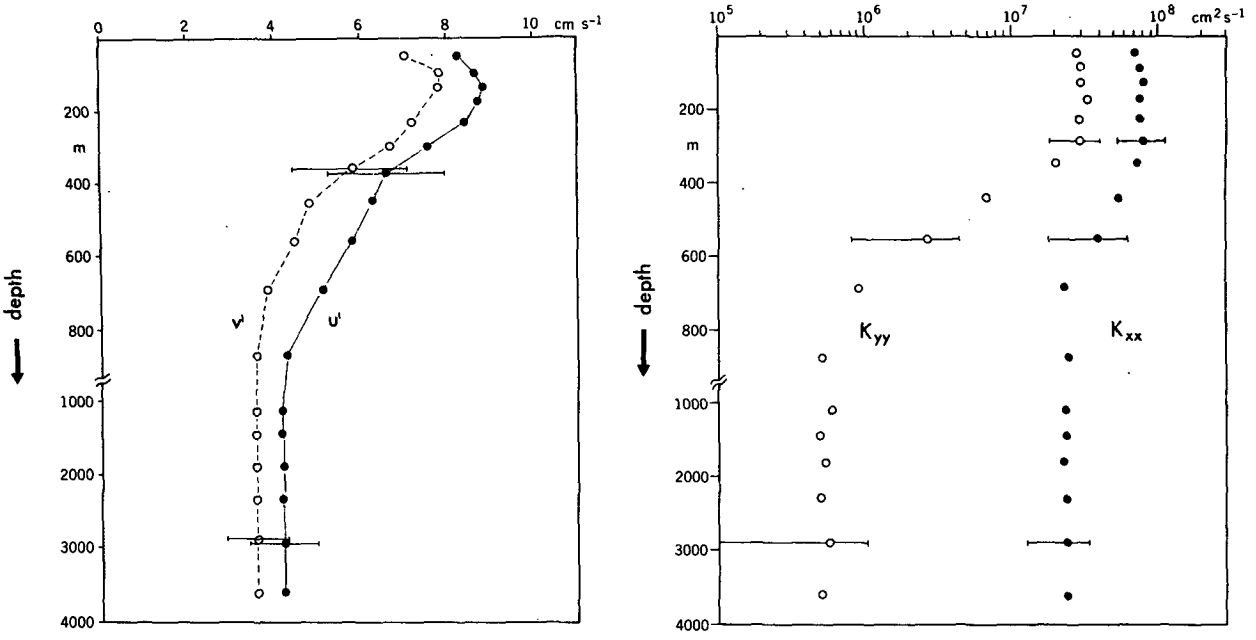

FIG. 12. Vertical profiles of velocity variances and of eddy diffusivities in the subtropical gyre (group A).

d. Dispersal characteristics in other areas

It is beyond the scope of the present paper to attempt a detailed exploration of eddy transport mechanisms in other areas of the model flow, i.e., the feasibility of the "eddy diffusivity" concept. For illustrative purposes, however, it may be instructive to look at some characteristic features of particle behavior in kinematically different regimes. The foregoing remarks (section 5b) with regard to the critical assumption of homogeneity should caution, however, against a quantitative interpretation.

Figure 14 shows correlation functions of ensembles in areas of comparatively high and low eddy energy, i.e., in the central eastward current and in the subpolar gyre. While in the former case zonal and meridional correlation functions are not very different and decrease rapidly, substantial differences between the components exist in the latter. The behavior seems to be another manifestation of the relatively more turbulent or wavelike behavior in weak and strong variability regions. The effect of the barotropic bands, only weakly dissipated while radiated away from the main instability areas, will be felt more strongly in the quieter parts of the basin.

We get a similar impression from the differences in dispersion. To illustrate this behavior we depict the geographical variation of Lagrangian diffusivities, defined in a similar way as above. (Note, again the cautionary remarks given before: in general, these values cannot be interpreted in terms of "eddy diffusivities"; they give, however, a good indication of the variation in the character of particle spreading.) Figure 15 gives a meridional section of K_{xx} and K_{yy} along, approximately, 35° longitude. Arrows along the top indicate the centers of the particle ensembles on which this compilation is based.

Highest values of K are concentrated in the subtropical thermocline, which is the main instability region in the model interior according to Cox's (1985) analysis. Anisotropy of particle spreading, increases both with depth and latitude, coincident with a decrease of eddy kinetic energy (Fig. 2 in Cox, 1985).

6. Discussion

The numerical experiment of Cox (1985) showed some interesting results of the effects of eddy mixing on property distributions in the thermocline. The significance of the primitive equation (PE) model lies in its inclusion of the thermohaline component of the circulation. In departure from quasi-geostrophic studies, the model includes the outcropping of isopycnal surfaces. Bryan (1987) points out the fundamental differences in the pattern of isopycnal potential vorticity that arise from this generalization, and notes various common features with oceanic fields in the PE case; i.e., the character of the homogenized regions. As noted earlier, the PE model contains essential elements of both RY and LPS theories; its results depart, however, from their assumption of a weak mixing. The model gives the impression of a circulation in which subducted fluid is rapidly mixed on its path into the gyre interior. The large homogenized areas of tracer and q in the model thermocline appear as consequences of a rather strong eddy mixing, differing from the ideal fluid as-

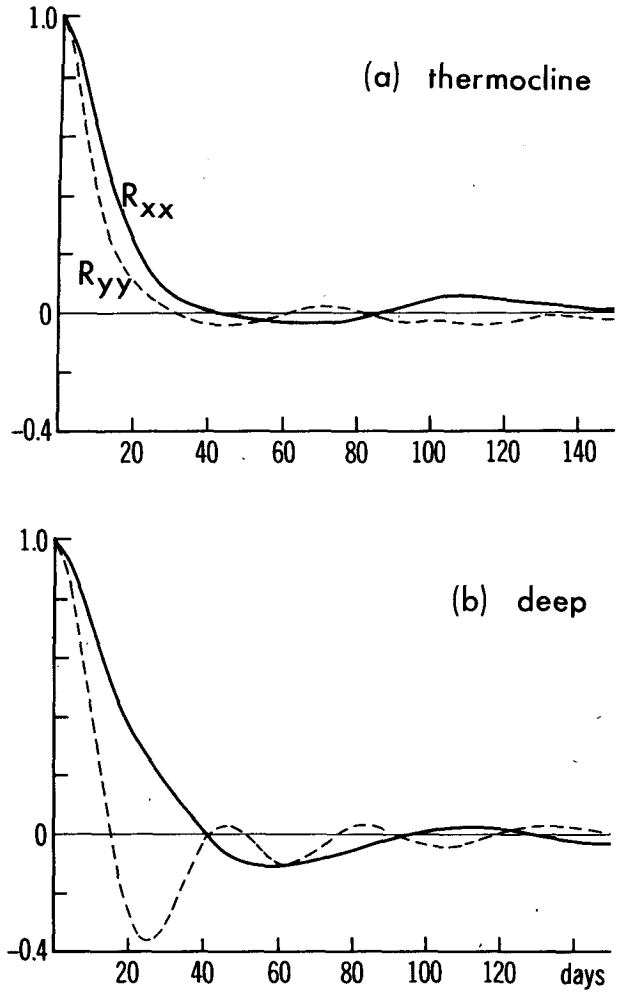

FIG. 13. Lagrangian velocity autocorrelation functions R_{xx} and R_{yy} (dashed) in the subtropical gyre (group A), starting levels (a) 90 m and (b) 1414 m.

sumptions of previous theoretical studies. In order to infer the significance of the diffusion properties revealed in the present study, we need to determine how the eddy characteristics relate to the real ocean.

a. Eddy kinetic energy

Some cautionary remarks are necessary. The model, with its simplified geometry and forcing patterns, cannot be regarded, and is not meant, as a simulation of a real ocean basin. The horizontal resolution of roughly 40 km allows only the representation of the upper range of mesoscale variability.

Within this context, a detailed comparison of the geophysical distribution of eddy variability would not be appropriate. A general feature of the eddy kinetic energy pattern, which this study seems to have in common with other models, (e.g., Holland et al., 1984) is worth noting, however, because it points to a specific problem which has to be addressed in future work. In the present primitive equation (Cox, 1985), as well as in quasi-geostrophic studies (Holland et al., 1983), basically three regions of eddy generation have been identified: the western boundary current/eastward jet region and its tight recirculation, and the westward return flow on the southern flank of the subtropical gyre. In the interior or eastern part of the basin, the eddy intensity decreases northward from moderate values in the subtropics to small or even very small values in the eastward flow associated with the boundary between the subtropical and subpolar gyre. Away from the western boundary, only the westward flowing portion of the gyre is found to be baroclinically unstable. (Note, however, that this signature is only apparent in model basins which are wide enough that the eastward penetration of the "Gulf Stream" jet with its associated high eddy activity is not a large fraction of the total width.) The meridional variation of K_E in the North Atlantic (NA) is found to be just the reverse: in its central/eastern part, eddy intensity systematically increases northward toward a maximum in the NA Current (Gould, 1983; Dickson, 1983; Krauss and Käse, 1984; Krauss and Böning, 1987). The mechanism of eddy generation in the eastward NA drift is an open question. While Krauss and Käse attributed this increase to an instability of the NAC, Dickson suggested that a significant part of it is contributed by direct atmospheric forcing on seasonal and synoptic scales. The effects of real basin geometry and forcing patterns, and the synoptic variability of atmospheric forcing have not been explored in eddy-resolving models as yet.

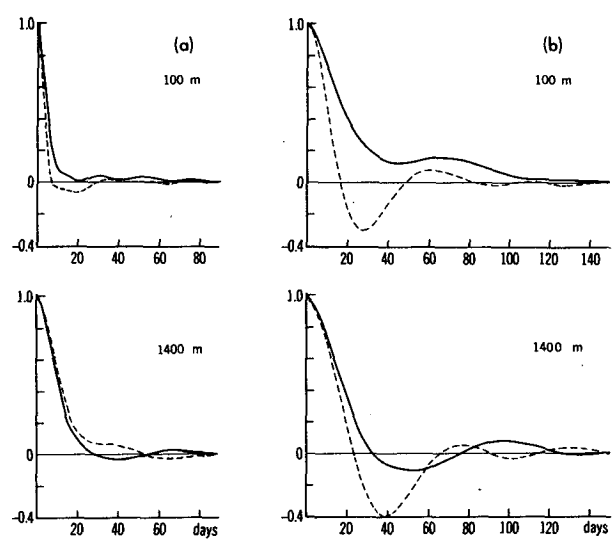

FIG. 14. Lagrangian velocity autocorrelation functions for a group in the midlatitude eastward jet (left column) and in a weak eddy field in the subpolar gyre (right column).

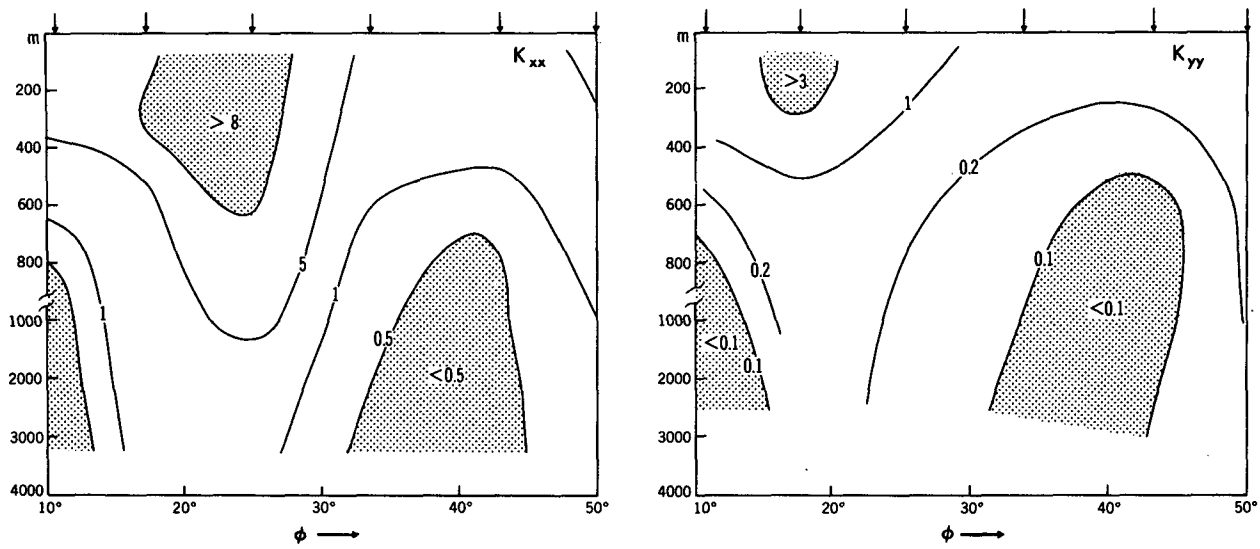

FIG. 15. Eddy diffusivities K_{xx} and K_{yy} for an approximately meridional section along $\lambda = 35°$. The arrows at the top indicate the mean positions of the groups used.

A main drawback in attempting a model/data comparison of eddy statistics in the central/eastern basin is the sparsity of data in these areas of the world ocean (Dickson, 1983). Wyrtki et al. (1976) have provided a representation of the world ocean's kinetic energy field using ship-drift data. Various problems with this type of database have, however, been noted (Wunsch, 1981). In the central/eastern ocean basins it leads to significantly higher K_E than revealed by direct, drifting buoy or current meter observations (e.g., Richardson, 1983). Though the model might in some sense be more representative of the North Pacific (e.g., see the K_E pattern derived from altimeter data by Cheney et al., 1983), a comparison with data has to rely mainly on NA observation.

Presently, the most comprehensive coverage of the eddy field at the surface of the central/eastern NA is provided by satellite-tracked drifting buoys. Krauss and Käse (1984) derived K_E values below 100 cm^2 s^{-1} south of about 40°N, increasing to typical values of 300 cm^2 s^{-2} along the path of the NAC. An extended database, used by Krauss and Böning (1987), confirmed this pattern; minimum values of 67 cm^2 s^{-2} were obtained at about 30°N.

The information from drifting buoys is complemented by a few current meter records, collected and discussed by Dickson (1983) and Gould (1983). Values of K_E in the thermocline (averaged over current meters between 0 and 800 m) are generally less than 100 cm^2 s^{-2} in the subtropical eastern NA. A general increase in these values is found north of 40°N. The "quiet" of much of the eastern basin is only relative, however, since K_E/K_M values are generally higher than 10, indicating that eddy variability still dominates the total flow.

Apart from the fact that the model fails to predict the northward increase of K_E, the eddy intensity in the subtropical thermocline may well be regarded as comparable to observed values. In deeper layers, however, the model K_E seems generally too high, though a considerable variability in the vertical structure has been revealed by the current meter records (Dickson, 1983). A model experiment on the effects of a rough bottom topography (Böning, 1987) indicates that the K_E level below the thermocline is very sensitive to eddy-topography interaction; on the other hand, the eddy intensity in the thermocline is not significantly different from the flat bottom case.

b. *Eddy mixing in the subtropical thermocline*

Diffusivity estimates for the area under consideration are even more sparse than information on K_E. Reassuringly, however, quite different approaches seem to give a consistent picture. From surface drifter dispersion, Krauss and Böning (1987) derived K_{xx}, K_{yy} of 2.5, 2.1 ($\times 10^7$ cm^2 s^{-1}) at 30°N, increasing northward almost linearly with eddy rms-velocities. Modeling observed tracer distributions on isopycnal surfaces (σ = 26.5 and 26.8) with a prescribed climatological mean flow, Thiele et al. (1986) derived eddy diffusivities of 2.9×10^7 cm^2 s^{-1} north, and 1.7×10^7 cm^2 s^{-1} south of 29°N as "best fit" values. Their values seem to agree with estimates of Armi and Stommel (1983), obtained by balancing salinity and oxygen advection against diffusion in their β-triangle. On a deeper level (σ = 27.1), they found $K = 5 \times 10^6$ cm^2 s^{-1}, with an increasing tendency towards shallower levels.

Our model results, with about 7 or 8 ($\times 10^7$), 3×10^7 cm^2 s^{-1}, seem to be generally higher than the observed

ones, 2–3 ($\times 10^7$ cm^2 s^{-1}) in the shallow thermocline, at least in the zonal component. Part of this may be attributed to the slightly larger K_E in this model area; however, a systematic difference from actual particle behavior in the ocean may arise from the absence of subsynoptic scales due to the grid size and the damping effect of the biharmonic friction in the model. One would expect such motions to shorten the decorrelation scales of Lagrangian time series, i.e., leading to smaller mixing lengths.

However, the somewhat higher model diffusivity does not necessarily mean a stronger effect of eddy mixing than in the oceanic thermocline. The tracer transport mechanism is probably better characterized by the relative influence of diffusive and advective effects. Thiele et al. (1986), taking a typical mean flow velocity of 1 cm s^{-1}, reported a "local" Péclèt number (based on L = 300 km) of 2 which is actually smaller than the model values of 3–4 in the upper thermocline. There is no doubt that advection has to be regarded as the dominant transport mechanism at larger scales; however, the model shows that this "local"eddy mixing is effective enough to shape significantly and, eventually, homogenize the distributions of passive tracers and q even on a gyre scale. The similar diffusion/advection ratio in the NA thermocline suggest that a similar mechanism may be accounted for in the formation of the oceanic tracer pattern.

c. *The anisotropy of deep particle dispersion*

A striking model feature is the large anisotropy of particle spreading in the subthermocline levels. We have pointed out earlier that this behavior can be attributed to the zonally oriented, bandlike structure which characterizes the low-frequency barotropic flow (Cox, 1987). The dispersion of fluid particles, after longer spreading times, is mainly influenced by the low-frequency part of the velocity spectrum (Kampé de Fériet, 1939). Since there exists only very limited Eulerian (current meter) information on the oceanic low-frequency variability, the characteristics of particle dispersion can provide a useful diagnostic for evaluating the model behavior against observations.

Information about the quasi-Lagrangian flow structure at the base and below the themocline are provided by SOFAR floats. The dispersion has been analyzed for some float ensembles in the western NA. Freeland et al. (1975) obtained Lagrangian diffusivities (K_x, K_y) = (0.78, 0.71) $\times$ 10^7 cm^2 s^{-1} from deep floats (1500 m) in the very calm MODE area, Rossby et al. (1983) reported (1.5, 1.5) $\times$ 10^7 cm^2 s^{-1} for 1300 m floats in the more energetic LDE area, Riser and Rossby (1983) obtained (0.9, 0.26) $\times$ 10^7 cm^2 s^{-1} with 2000 m POLYMODE floats. An important feature in terms of the present analysis is that the observed spreading in the deep ocean is of much more isotropic character than the spreading of the model particles. This comparison suggests that the effect of the low-frequency, zonal motions is too strong in the present model.

The sensitivity experiment with bottom topography (Böning, 1987) shows that a rough bottom floor, in addition to strongly affecting the barotropic flow component, has a significant impact on particle spreading in the deeper levels, leading to a much more isotropic behavior. On the other hand, thermocline particles were not found to react sensitively; in this respect, our conclusions drawn here are not affected by the results of the bottom topography experiment.

7. Conclusions

The eddy-resolving, primitive equation model of Cox (1985) demonstrated a strong effect of eddy mixing on distributions of conservative properties in the interior of the subtropical thermocline. We have used a Lagrangian approach to examine the diffusive behavior of the flow field in this region. The spreading of fluid particles illustrates in a direct way the relative importance of advective and diffusive mechanisms in transporting passive tracers or potential vorticity along isopycnal surfaces from the outcrop line into the interior.

During the first few months of particle motion, eddy displacements are of the same order of magnitude as the displacement by the mean flow. While in general, especially near boundary currents, the inhomogeneity of the oceanic flow field may be too strong for this concept to hold, an "eddy diffusivity" seems to be applicable in the interior portion of the subtropical gyre. Single particle dispersion follows a random walk behavior between 30 or 40 and 100 days, leading to a constant Lagrangian diffusivity K during this period. After about 100 days, alongflow dispersion was seen to increase sharply, indicating the influence of shear dispersion which is assumed to become dominant for longer periods.

Diffusivity values were then defined as the time mean of $K(t)$ between days 40 and 100 and averaged over ten realizations with ensembles consisting of 144 particles in each of the 18 model levels. They decreased from thermocline values of (K_{xx}, K_{yy}) = (8×10^7, 3×10^7 cm^2 s^{-1}) to almost depth-independent values of 2×10^7, 1×10^6 cm^2 s^{-1} below the thermocline. The strong anisotropy of particle spreading in the deep model levels is consistent with an Eulerian signature of zonally oriented bands of low-frequency, barotropic motions, discussed by Cox (1987). The model anisotropy appears to be too strong, however, when compared with the observed behavior of deep SOFAR floats, indicating a major model problem in simulating the vertical structure of the oceanic variability.

Since the numerical model includes both ventilated and recirculating aspects of the oceanic subtropical circulation, it combines elements of the RY and LPS the-

ories. In contrast to the assumption of an almost inviscid, q conserving flow, the model solution is characterized by rather strong eddy mixing. Both mean advection and diffusion are important transport mechanisms in the gyre interior. Particles are seen to disperse rapidly, covering a large fraction of the gyre before being advected around with the mean flow. The model thus illustrates a case where homogenization of passive tracers or q occurs without obeying the "weak mixing" requirement of RY's theory. However, Rhines (1986) pointed out that homogenization within a gyre could occur also with a rather "strong" eddy diffusivity in the interior, as long as inward mixing of nonuniform tracer values across the rim of the gyre would be small. It seems that even the moderate eddy activity in the gyre interior is sufficient to mix effectively the plume of entering, "ventilated" water with the pool of recirculating, "older" water in the thermocline.

Notwithstanding its various problems, i.e., by accurately simulating the geographical distribution of eddy variability, the model illustrates the role which locally strong eddy mixing may play in shaping the fields of passive tracers in the oceanic thermocline. With observed Péclèt numbers actually smaller in the "quiet" region of the eastern subtropical North Atlantic, the model strongly suggests that the assumption of an "almost ideal" fluid might not be appropriate when considering tracer transport in the ocean.

Acknowledgments. We are deeply grateful to Kirk Bryan for his encouragement and continued interest during the development of this work. Thanks also to Messrs. Philip Tunison and John Conner for their assistance in drafting the figures and Ms. Johann Callan for the preparation of the manuscript. One of us (C.W.B.) is supported at the Geophysical Fluid Dynamics Program by NOAA Grant NA84EAD00051.

REFERENCES

Armi, L., and H. Stommel, 1983: Four views of a portion of the North Atlantic subtropical gyre. *J. Phys. Oceanogr.*, **13**, 828–857.

Batchelor, G. K., 1949: Diffusion in a field of homogeneous turbulence. I. Eulerian Analysis. *Aust. J. Sci. Res.*, **A2**, 437–450.

Böning, C. W., 1987: Influences of a rough bottom topography on flow kinematics in an eddy-resolving circulation model. *J. Phys. Oceanogr.*, submitted.

Bryan, K., 1987: Potential vorticity in models of the ocean circulation. *Quart. J. Roy. Meteor. Soc.*, submitted.

Cheney, R. E., J. G. Marsh and B. D. Beckley, 1983: Global mesoscale variability from collinear tracks of SEASAT altimeter data. *J. Geophys. Res.*, **88**, 4343–4354.

Colin de Verdiere, A., 1983: Lagrangian eddy statistics from surface drifters in the eastern North Atlantic. *J. Mar. Res.*, **41**, 375–398.

Corrsin, S., 1959: Progress report on some turbulent diffusion research. *Advances in Geophysics*, Vol. 6, Academic Press, 161–164.

——, 1974: Limitations of gradient transport models in random walks and in turbulence. *Advances in Geophysics*, Vol. 18A, Academic Press, 25–56.

Cox, M. D., 1985: An eddy resolving numerical model of the ventilated thermocline. *J. Phys. Oceanogr.*, **15**, 1312–1324.

——, 1987: An eddy resolving numerical model of the ventilated thermocline: Time dependence. *J. Phys. Oceanogr.*, **17**, 1044–1056.

——, and K. Bryan, 1984: A numerical model of the ventilated thermocline. *J. Phys. Oceanogr.*, **14**, 674–687.

Davis, R. E., 1983: Oceanic property transport, Lagrangian particle statistics, and their prediction. *J. Mar. Res.*, **41**, 163–194.

Deardorff, J. W., and R. L. Peskin, 1970: Lagrangian statistics from numerically integrated turbulent shear flow. *Phys. Fluids*, **13**, 584–595.

Dickson, R. R., 1983: Global summaries and intercomparison: Flow statistics from long-term current meter moorings. *Eddies in Marine Science*, A. R. Robinson, Ed., Springer Verlag.

Freeland, H. J., P. Rhines and H. T. Rossby, 1975: Statistical observations of trajectories of neutrally buoyant floats in the North Atlantic. *J. Mar. Res.*, **33**, 383–404.

Gould, W. J., 1983: The Northeast Atlantic Ocean. *Eddies in Marine Science*, A. R. Robinson, Ed., Springer Verlag.

Haidvogel, D. B., 1982: On the feasibility of particle tracking in Eulerian ocean models. *Ocean Modelling* (Unpublished manuscript), **45**, 4–9.

——, 1984: Particle dispersion and Lagrangian vorticity conservation in models of β-plane turbulence. (Unpublished manuscript)

Harrison, D. E., 1978: On the diffusion parameterization of mesoscale eddy effects from a numerical ocean experiment. *J. Phys. Oceanogr.*, **8**, 913–918.

Holland, W. R., D. E. Harrison and A. J. Semtner, Jr., 1983: Eddy-resolving numerical models of large-scale ocean circulation. *Eddies in Marine Science*, A. R. Robinson, Ed., Springer Verlag, 609 pp.

——, T. Keffer and P. B. Rhines, 1984: Dynamics of the oceanic general circulation: The potential vorticity field. *Nature*, **308**, 698–705.

Holloway, G., and S. S. Kristmannsson, 1984: Stirring and transport of tracer fields by geostrophic turbulence. *J. Fluid Mech.*, **141**, 27–50.

Hsu, C.-P. F., 1980: Air parcel motions during a numerically simulated sudden stratospheric warming. *J. Atmos. Sci.*, **37**, 2768–2792.

Kampé de Fériet, J., 1939: Les fonctions aléatoires stationnaires et la théorie statistique de la turbulence homogène. *Ann. Soc. Sci. Bruxelles*, **59**, 145–194.

Keffer, T., 1985: The ventilation of the world's oceans: Maps of the potential vorticity field. *J. Phys. Oceanogr.*, **15**, 509–523.

Kida, H., 1983: General circulation of air parcels and transport characteristics derived from a hemispheric GCM. Part 1. A determination of advective mass flow in the lower stratosphere. *J. Meteor. Soc. Japan*, **61**, 171–187.

Krauss, W., and R. H. Käse, 1984: Mean circulation and eddy kinetic energy in the eastern North Atlantic. *J. Geophys. Res.*, **89**, 3407–3415.

——, and C. W. Böning, 1987: Lagrangian properties of eddy fields in the northern North Atlantic as deduced from satellite-tracked buoys. *J. Mar. Res.*, **45**, 259–291.

Luyten, J. R., J. Pedlovsky and H. Stommel, 1983: The ventilated thermocline. *J. Phys. Oceanogr.*, **13**, 292–309.

McDowell, S., P. B. Rhines and T. Keffer, 1982: North Atlantic potential vorticity and its relation to the general circulation. *J. Phys. Oceanogr.*, **12**, 1417–1436.

Monin, A. S., and A. M. Yaglom, 1971: *Statistical Fluid Mechanics, Vol. 1,* J. L. Lumley, Ed., The MIT Press, 769 pp.

Rhines, P. B. 1986: Vorticity dynamics of the oceanic general circulation. *Annual Reviews in Fluid Mechanics,* Vol. 18, Annual Reviews 433–497.

——, and W. Young, 1982: A theory of wind-driven ocean circulation, I. Mid-ocean gyres. *J. Mar. Res.,* **40**(Suppl.), 559–596.

Richardson, P. L., 1983: Eddy kinetic energy in the North Atlantic from surface drifters. *J. Geophys. Res.,* **88,** 4355–4367.

Riley, J. J., and S. Corrsin, 1974: The relation of turbulent diffusivities to Lagrangian velocity statistics for the simplest shear flow. *J. Geophys. Res.,* **79,** 1768–1771.

Riser, S. C., and H. T. Rossby, 1983: Quasi-Lagrangian structure and variability of the subtropical western North Atlantic circulation. *J. Mar. Res.,* **41,** 127–162.

Rossby, H. T., S. C. Riser and A. J. Mariano, 1983: The western North Atlantic—A Lagrangian viewpoint. *Eddies in Marine Science,* A. R. Robinson, Ed., Springer Verlag, 609 pp.

Sarmiento, J. L., 1983: A tritium box model of the North Atlantic thermocline. *J. Phys. Oceanogr.,* **13,** 1269–1274.

Taylor, G. I., 1921: Diffusion by continuous movements. *Proc. London Math. Soc.,* Ser. 2, Vol. 20, 196–212.

Thiele, G., et al., 1986: Baroclinic flow and transient-tracer fields in the Canary–Cape Verde Basin. *J. Phys. Oceanogr.,* **16,** 814–826.

Wunsch, C., 1981: Low-frequency variability in the sea. *Evolution of Physical Oceanography,* B. A. Warren and C. Wunsch, Eds., The MIT Press, 623 pp.

Wyrtki, K., L. Magaard and J. Hager, 1976: Eddy energy in the oceans. *J. Geophys. Res.,* **81,** 2641–2646.